Available online at www.sciencedirect.com
SCIENCE DIRECT
Journal of Catalysis 230 (2005) 109–122
JOURNAL OF CATALYSIS
www.elsevier.com/locate/jcat

Ketonization of acetic acid vapour over polycrystalline magnesia: in situ Fourier transform infrared spectroscopy and kinetic studies

G.A.H. Mekhemer [a], S.A. Halawy [b], M.A. Mohamed [b], M.I. Zaki [a,*]

[a] *Chemistry Department, Faculty of Science, Minia University, El-Minia 61519, Egypt*
[b] *Chemistry Department, Faculty of Science, South Valley University, Qena 83523, Egypt*

Received 15 July 2004; revised 26 September 2004; accepted 28 September 2004

Abstract

Ketonization of acetic acid vapour over polycrystalline MgO was examined both kinetically and spectroscopically from room temperature to 480 °C. The kinetic study was performed with the use of a flow-reactor and gas chromatography, whereby the reaction rate and the catalyst selectivity were determined. The spectroscopic study was carried out by means of in situ infrared (IR) absorption measurement. Nature and products of adsorptive and absorptive interactions with the catalyst not only of the acid, but also of products of the reaction (acetone and CO_2) were identified by in situ IR spectroscopy, and quantified by thermogravimetric analysis. Moreover, adsorption and surface reactions of methylbutynol molecules were observed by IR spectroscopy and utilized to probe specifically the availability on MgO surfaces of strong, reactive base (O^{2-}) sites. The results could help to reveal the strong catalyst tendency towards absorption of the acid and CO_2 molecules, and consequent formation of magnesium acetate and carbonate bulk phases, respectively. This unexpected behaviour of MgO, which enjoys high lattice (Mg–O bond) energy, was considered to be driven by the strong catalyst basicity (ionicity). Accordingly, the ketonization of acetic acid over MgO was found to occur via overlapping catalytic and pyrolytic routes. Reactive species and reaction pathways involved in each route were proposed.

Keywords: Acetic acid ketonization; Magnesium oxide ketonization catalyst; Ketonization reactive surface and bulk species; Ketonization mechanism; In situ infrared spectroscopy

1. Introduction

Ketonization (decarboxylative coupling) of alcohols [1], esters [2–4], or carboxylic acids [1,5–8] is originally a biological process [9,10] that has long been successfully simulated at the laboratory level to produce saturated and unsaturated ketones of industrial and technological importance. Whether performed in the gas phase [5,6,11,12], in solution [13], or in the solid state [14–16], ketonization is carried out catalytically [5,6,17,18], pyrolytically [14–16], or photolytically [19–21]. It is considered a more efficient utilization of wastes of technical fatty acids [2] and wood products [22], and a more effective synthesis of ketones from natural oil [23]. Moreover, its primary ketonic products are basic chemicals for the fabrication of a variety of polymers, which, when thermochemically condensed or sulfonated, produce widely used metal coatings [24] and wetting and emulsifying agents [25].

It is worth mentioning, however, that catalytic ketonization of carboxylic acids has been considered simpler, more economic, and more versatile than both the pyrolytic and photolytic means of ketonization [5]. In biological systems, ketonization is homogeneously (enzymatically) catalyzed [9,10], but in nonbiological systems it is largely heterogeneously catalyzed. A large variety of heterogeneous oxidic catalysts have been tested and found to be ketonization-competent (e.g., [5–9]), but only a few, namely, catalysts based on oxides of manganese [8,11,12], thorium [17,26], cerium [5], and Na-mordenite [27], have been capable of

* Corresponding author. Fax: +20 86 2360833.
E-mail address: mizaki@link.net (M.I. Zaki).

0021-9517/$ – see front matter
doi:10.1016/j.jcat.2004.09.030

bringing the reaction temperature down to < 300 °C. If the primary ketonic products were the sought ketonization yield, it is, therefore, crucial to have the reaction proceed at a lower temperature than that (> 400 °C) at which pyrolytic and/or surface secondary reactions of the gas phase products are often triggered [28,29].

Previous research investigations of catalytic ketonization of carboxylic acids have most frequently been kinetic studies, and have rarely been in situ spectroscopic studies [5,18]. A wide range of reaction variables have thereby been examined, including carboxylic acid chain length [8,17] and branching [30], reaction dynamics [7], and catalyst surface chemistry [5,13,18], texture [11], and structure [31]. The results obtained could reveal that a straightforward, facile ketonization is only possible when nonbranching carboxylic acids of short chain length are used. Moreover, metal oxide catalysts exposing Lewis acid sites of different coordination unsaturations (namely, five- and four-fold coordinated) [31] with reversible redox properties [5], or coordinatively unsaturated Lewis base sites and proton-donor centers [13], are most active and selective.

Mechanistically speaking, however, catalytic ketonization of gas-phase carboxylic acids have been suggested [32] to follow the Langmuir–Hinshelwood model rather than the Eley–Rideal model. Recently the ketonization process has consistently been proposed to be a bimolecular, second-order reaction between surface carboxylate species [7]. According to Pestman et al. [7], this is only true if the reaction is carried out under nonstationary conditions. Otherwise, under stationary conditions there is the possibility of partial conversion of the oxide catalyst into bulk carboxylate, which would subsequently lead to pyrolytic and/or catalytic–pyrolytic ketonization at the solid–solid oxide/carboxylate interface thus established [7]. Metal oxides of low lattice energy (i.e., dwelling weak metal–oxygen bonds) have been believed to favor the latter mechanistic pathway [7].

With the above experimental and mechanistic considerations in mind, the present investigation was designed to examine the ketonization of acetic acid vapour over polycrystalline MgO catalyst, with the use of both flow and stationary reactors, in the hope of gaining a deeper insight into the mechanism of the reaction pathways. In a flow reactor, the gas-phase reaction mixture (reactant + product(s)) was separated and quantified by means of an on-line gas chromatograph; the gas-phase and adsorbed species formed in a stationary reactor were in situ characterized by Fourier transform infrared (FTIR) spectroscopy. The reactant acid chosen, CH_3COOH, is significantly stable to pyrolysis over the test reaction-temperature regime (room temperature (RT) to 480 °C) [5] and, furthermore, is short and nonbranching, indicating a straightforward ketonization [33]: $2CH_3COOH \rightarrow CH_3COCH_3 + CO_2 + H_2O$. The test catalyst, MgO, is a typical basic oxide; its polycrystalline nature facilitates exposure on the surface of variously coordinated Mg^{2+} and O^{2-} sites [34–38], whereas the ionic nature of its bulk structure ought to warrant a high lattice energy and, consequently, no tendency toward formation of bulk acetates [7]. Nevertheless, thermogravimetry was used to explore the catalyst absorption capacity toward the reactant molecules and possible formation of bulk acetate species. Moreover, IR spectroscopy was used to examine adsorption and surface reactions of various probe molecules (namely, methylbutynol, acetone, and CO_2) to assess the nature of the active sites exposed on the catalyst surface, as well as further surface reactions of the acetic acid ketonization products (acetone and CO_2).

2. Experimental

2.1. Materials

2.1.1. The catalyst

Polycrystalline MgO was obtained by calcination (heating in a static atmosphere of air) of a home-made magnesium oxalate dihydrate ($MgC_2O_4 \cdot 2H_2O$) at 600 °C for 4 h. The parent oxalate compound was prepared, with a procedure similar to that used previously to prepare copper oxalate [39]. Particles of a basic magnesium carbonate compound ($Mg_4(CO_3)_3(OH)_2 \cdot 3H_2O$, AR-grade Prolabo product, France) were sprinkled onto a 0.3 M aqueous solution of oxalic acid ($H_2C_2O_4 \cdot 2H_2O$, AR-grade Aldrich product, USA) with continuous stirring and heating at 50 °C until effervescence of CO_2 ceased. The white precipitate thus formed (the oxalate compound) was left to settle at 50 °C for 12 h, filtered off, washed thoroughly with distilled water, and heated at 100 °C until complete dryness.

A previous characterization of the MgO thus obtained [35] found the material bulk to assume the crystalline structure of Periclase-type cubic MgO (JCPDS 4-0829) [40] and to comprise fine particles with an average crystallite size of 7 nm. Furthermore, the material surface was found to assume a specific surface area of 91 m^2/g and to expose weak Lewis acid sites, associated essentially with five- and four-fold coordinated Mg^{2+} sites; strong basic sites, associated with surface-OH groups bound linearly to Mg^{2+} sites; and coordinatively unsaturated O^{2-} lattice sites.

2.1.2. The reactant

Reactant molecules (CH_3COOH; denoted AcOOH) were provided by expanded vapours of liquid glacial acetic acid (99% pure product of J.T. Baker, Holland). The source liquid was deaerated before use with in situ FTIR experiments (vide infra) by on-line freeze–pump–thaw cycles performed at liquid nitrogen temperature (−195 °C). In the vapour phase the AcOOH molecules are dimerized and stable to pyrolysis up to 480 °C [5].

2.1.3. Infrared probe molecules

In addition to AcOOH molecules, those of methylbutynol ($((CH_3)_2C(OH)C{\equiv}CH$; denoted MBOH), acetone ($((CH_3)_2C{=}O$; denoted Ac), and CO_2 were used as IR

probes. The MBOH and Ac molecules were provided by expanded vapours of corresponding source liquids (AR-grade products of Aldrich, USA), whereas the CO_2 molecules were provided by 99.99% pure, Merck carbon dioxide gas (Germany). The source liquids were deaerated before application by on-line freeze–pump–thaw cycles performed at liquid nitrogen temperature, whereas the source gas was applied as supplied.

2.1.4. In situ treatment gases

Oxygen (O_2), nitrogen (N_2), and air used to furnish the atmosphere for in situ thermal treatments and thermogravimetry were 99% pure products from the Egyptian Company of Industrial Gases (El-Hawamdyia, Egypt). Prior to application they were further purified by passage through liquid nitrogen-cooled traps.

2.2. Apparatus and techniques

2.2.1. Thermogravimetry

Thermogravimetry (TG) analysis was performed on small portions (10–15 mg) of test MgO samples (before and after a 2-h exposure to AcOOH vapour at RT) while they were heated (at 20 °C/min) in a dynamic gas atmosphere of air or N_2 (40 cm^3/min), with the use of a Shimadzu "Stand Alone" thermal analyzer equipped with a TGA-50H thermobalance and a TA-50WSI data acquisition and handling system (Japan).

2.2.2. Infrared spectroscopy

Ex situ and in situ IR spectra were recorded over the frequency range 4000–400 cm^{-1}, with a model Genesis-II FTIR Mattson spectrometer (USA) and an on-line PC with WinFIRST Lite (v1.02) software for spectra acquisition and handling. The ex situ spectra were taken of lightly loaded (< 1 wt%), thin discs of KBr-supported test samples (average 10 scans at 2.0 cm^{-1} resolution).

The in situ spectra were taken (average 100 scans at 2.0 cm^{-1} resolution) of self-supporting, thin wafers of the catalyst ($\sim$ 30 mg/cm^2) mounted inside a specially designed Pyrex/quartz glass, high-temperature IR static reactor/cell [41], equipped with BaF_2 windows. The catalyst test wafer was first outgassed at RT and 10^{-5} Torr (1 Torr = 133.3 Pa), activated in a stream of O_2 (50 cm^3/min) at 450 °C for 1 h and, subsequently, outgassed at the same temperature and 10^{-5} Torr for 30 min. The temperature was then decreased to RT under a dynamic vacuum, the wafer and cell background spectra were acquired, and a certain dose (3–20 Torr) of either AcOOH, MBOH, Ac, or CO_2 gas-phase molecules was admitted into the cell. We maintained the gas/wafer interface at RT for 5 min before we: (i) recorded a spectrum of the wafer (*plus* gas phase, cell background, and adsorbed species); (ii) lifted the wafer and recorded a spectrum of the gas phase (*plus* cell background); (iii) pumped off the gas phase for 5 min; and (iv) took another spectrum of the wafer (*plus* adsorbed species and cell background). This sequence of measurements was repeated at higher temperatures (100–480 °C), and the spectra were measured after cooling to RT. Difference spectra of gas-phase and adsorbed species were obtained by absorption subtraction of the cell and wafer background spectra, with the use of the installed software.

2.2.3. Gas chromatography

AcOOH ketonization activity measurement was performed in a flow system equipped with an all-Pyrex glass, fixed-bed reactor and a model GC-14A Shimadzu gas chromatograph (Japan). The chromatograph was equipped with flame ionization (FID) and thermal conductivity (TCD) detectors; a PEG 6000 10% on Shimalite TPA, 60/80 mesh (2 m × 3 mm i.d.) column maintained at 140 °C; and a type HGS-2 heatable gas-sampling valve. The flow system was heated by means of a heating tape to at least 100 °C, to avoid condensation of both reactant and products. All runs were conducted at atmospheric pressure, with the use of 0.86% AcOOH in a stream (165.4 cm^3 (STP)/min) of dry N_2 and a prestabilized catalyst sample (50 mg) at 450 °C for 1 h, and measurements were undertaken during stepwise heating from RT up to 480 °C. To allow for a steady state, the AcOOH/catalyst interface was maintained at the set temperature for 5 min before gas samples were subjected to gas chromatography (GC) analysis. The recorded values of the peak areas were converted into gas concentrations with the use of sensitivity factors determined by calibration. Conversion (%), reaction rate (mmol h^{-1} g_{cat}^{-1}), and catalyst selectivity were calculated as detailed earlier [42]. It is worth mentioning that in a single exploratory attempt measurements were carried out on cooling from 480 °C down to RT. However, this mode of measurement was abandoned, for the initially white catalyst material was rendered grayish in color. A postanalysis of the catalyst revealed formation of carbonaceous deposits.

3. Results and discussion

3.1. AcOOH absorption capacity

The capacity of metal oxides to absorb AcOOH molecules and form bulk acetate compounds has been intimately related to the oxide lattice energy (the metal–oxygen bond strength) [43]. This relationship has been based on the generally higher thermodynamic stability of metal acetates compared with the corresponding metal oxides [43]. Accordingly, the present metal oxide catalyst (MgO), which is considered to be one of the oxides assuming high lattice energy [7], ought to exhibit no tendency toward absorption of AcOOH molecules. In contrast, Pestman et al. [7], through quantitative estimation of AcOOH gas phase over MgO as a function of temperature, have found indications of the occurrence of absorption and formation of bulk magnesium acetate. Therefore, we found it imperative in the present investigation to examine the MgO material itself before and

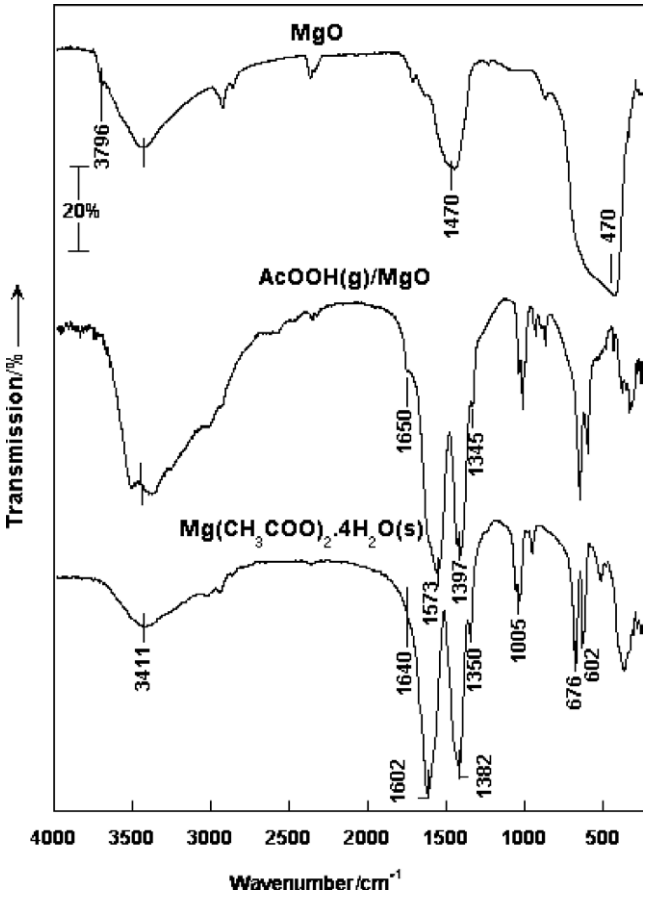

Fig. 1. Ex situ IR spectra taken at room (beam) temperature of KBr-supported samples of the materials indicated ($AcOOH_{(g)}/MgO$ = MgO following exposure to AcOOH vapour at RT for 2 h).

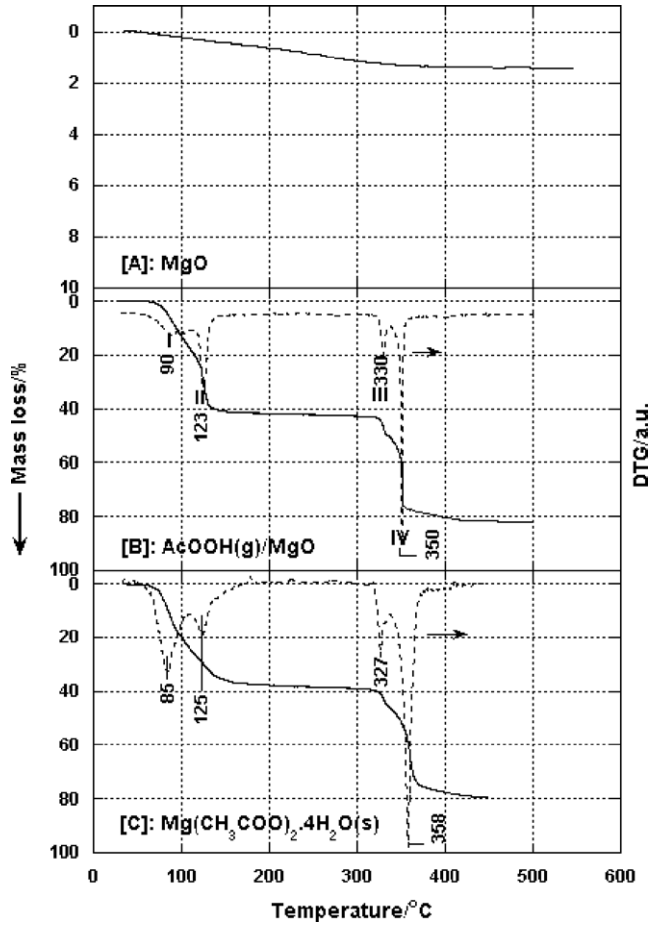

Fig. 2. TG (and DTG) curves exhibited on heating (at 20 °C/min) small portions (10–15 mg) of the materials indicated in the atmosphere of air (50 cm^3/min).

after exposure to an AcOOH atmosphere at RT for 2 h, using, respectively, IR and TG analyses for qualitative and quantitative assessments of the phenomenon.

The IR spectra (ex situ) obtained are compared in Fig. 1 with a spectrum exhibited by a commercial magnesium acetate compound. The comparison reveals beyond a doubt the conversion of MgO into acetate bulk phase by disclosing the complete disappearance of the very strong, broad IR absorption (centered around 470 cm^{-1}) due to lattice Mg–O bond vibrations [44] in the spectrum (labeled $AcOOH_g/MgO$) obtained following exposure to acid vapour. The latter spectrum displays instead two very strong absorptions at 1573 and 1397 cm^{-1}, assignable to antisymmetric and symmetric νCOO^- vibrations of acetate species [45], which are quite comparable to those monitored in the spectrum taken of the bulk $Mg(CH_3COO)_2 \cdot 4H_2O$ compound. Moreover, the two spectra exhibit similarly ill-defined absorptions (at 1650–1640 cm^{-1}) assignable to δOH vibrations of water molecules; very broad absorptions, centered around 3411 cm^{-1} and due to νOH vibrations of associated OH-groups [46]; and a set of sharp absorptions at $\leqslant$ 1005 cm^{-1} due to δC–H/νC–O/νC–C vibrations of the acetate species [45]. It is worth noting that the extra absorptions monitored at 3796 and 1470 cm^{-1} in the spectrum taken of MgO, before exposure to the acid atmosphere, are due respectively to νOH and νOCO vibrations of isolated surface hydroxyls and carbonate impurity species [47]. The fact that the νOH vibrations occur at a much higher frequency than that (3750–3740 cm^{-1}) reported [34] for νMgO–H exposed on pure magnesia surfaces, may be attributed to direct or indirect impacts of the sample support (KBr). The ex situ mode of measurement may relate, moreover, the observed association of OH groups (the absorption centered around 3411 cm^{-1}) to adsorption of atmospheric water molecules. δOH vibrations of H_2O molecules may still be resolved in the spectrum of MgO near 1650 cm^{-1}.

The question of whether the exposure to the AcOOH vapour quantitatively converted the MgO into bulk acetate compound was addressed by TG analysis of the oxide before and after exposure to the acid atmosphere. The TG and DTG (differential thermogravimetric analysis) curves obtained are compared in Fig. 2 with the curves exhibited by a commercial $Mg(CH_3COO)_2 \cdot 4H_2O$ compound. Whereas the oxide before exposure to the acid atmosphere is shown (Fig. 2A) to suffer only a minute mass loss ($\sim$ 1.5%) upon heating to 550 °C, most probably as a result of elimination of the IR-detected surface impurity species, a much larger

total mass loss (82.3%) is conceded by the oxide exposed to the acid atmosphere (Fig. 2B). Both the total mass loss and the four mass loss steps (steps I–IV) resolved in the corresponding TG and DTG curves (Fig. 2B) are very similar to those (81.5%; four steps) exhibited by the commercial acetate compound in Fig. 2C, although the observed total mass loss for the test acetates is very close to that (81.3%) expected for complete conversion into pure MgO. IR examination of the solid-phase acetate decomposition products at 250, 320, and 400 °C revealed the formation of intermediate anhydrous magnesium acetate following a two-step dehydration (steps I and II), which decomposes through step III into an intermediate basic magnesium carbonate and proceeds to the formation of pure MgO via the mass loss step (IV). This suggested that the thermal decomposition course is largely similar to that reported elsewhere [47], except for the sole formation of anhydrous acetate following steps I and II. Bernard and Busnot [47] have suggested, instead, the formation of a basic acetate phase. Although the observed mass loss via steps I and II (ca. 40%) is rather close to that (ca. 36%) expected for the elimination of the 4 moles of water, the ambiguity shrouding the molecular structure of the proposed basic acetate prevents us from excluding its formation. Hence, the TG results complement the IR results in disclosing the high AcOOH absorption capacity of MgO at RT. A quantitative conversion into a bulk compound of acetate tetrahydrate is feasible within 2 h at RT. This finding can lend strong support to the conclusions of Pestman et al. [7], who argued that the AcOOH absorption capacity of metal oxides is enhanced not only by the low lattice energy of the oxide, but also by the oxide basicity (ionicity). The following section may help us to probe the availability and reactivity of basic sites exposed on the test MgO catalyst.

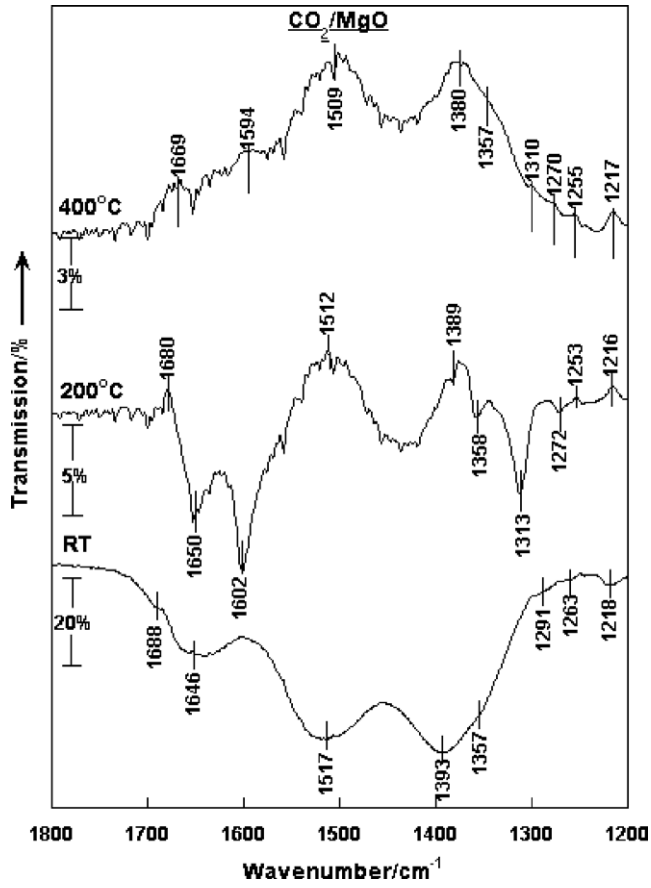

Fig. 3. In situ IR spectra taken at beam temperature of irreversibly adsorbed species of CO_2 on MgO at the temperatures indicated (the 200 and 400 °C spectra are difference spectra obtained following absorption subtraction of the RT-spectrum).

3.2. Surface site reactivities

3.2.1. CO_2/MgO

Fig. 3 compares three in situ IR spectra taken of CO_2/MgO over the νOCO frequency range (1800–1200 cm^{-1}); they are for the irreversibly adsorbed species at RT, 200 °C, and 400 °C. The RT spectrum displays three strong, broad absorptions centered around 1646, 1517, and 1393 cm^{-1}; two medium-to-strong shoulders at 1688 and 1357 cm^{-1}; and three tiny absorptions at 1291, 1263, and 1218 cm^{-1}. According to Busca and Lorenzelli [48], the frequencies and the obvious broadness of these absorptions suggest the formation of a mixture of carbonate and bicarbonate surface species. The peaks around 1517 and 1393 cm^{-1} are due, respectively, to ν_{as} and ν_sOCO vibrations of monodentate-bound carbonate species ($\Delta\nu = \nu_{as} - \nu_s < 200$ cm^{-1}) [48], whereas the high-frequency ν_{as}OCO peaks at 1688 and 1646 cm^{-1} are usually considered to be for bidentate-bound carbonate and/or bicarbonate species [48]. The corresponding ν_sOCO vibrations should occur respectively at 1350–1270 and 1450–1400 cm^{-1}; that is, they may still contribute to the large absorptions centered around 1517 and 1393 cm^{-1}.

The 200 and 400 °C spectra (Fig. 3) are difference spectra obtained following subtraction of the RT spectrum. The 200 °C spectrum shows retrogression of absorptions (negative peaks) at 1680, 1512, 1389, 1253, and 1216 cm^{-1} and persistence of absorptions (positive peaks) at 1650, 1602, 1358, 1313, and 1272 cm^{-1}. The weakened set of absorptions is due exclusively to bicarbonate and monodentate carbonate species [48,49], whereas the persistent set of absorptions is due to bidentate carbonate species [47]. In a recent investigation [35], deconvolution of a similar IR spectrum, taken of CO_2/MgO, resolved weak νOCO absorptions (at 1591, 1523, 1497, and 1456 cm^{-1}) assignable to bulk-like carbonate species. Occurrence of such absorptions in the present spectra would be consistent with the IR-implied tendency of MgO to absorb CO_2 and form bulk carbonate species (Fig. 3) and, therefore, cannot be excluded with certainty. Upon a further increase of temperature to 400 °C, the difference spectrum obtained (Fig. 3) shows a progressive indiscriminate weakening of all of the absorptions observed initially in the RT spectrum. This indicates clearly that not

only surface carbonate species (Figs. 2B and C) but also bulk-like carbonates are largely destabilized at 400 °C.

Within the context of the present work, the above results may support the following conclusions: (i) the irreversible adsorption of the weakly acidic CO_2 molecules on MgO at RT reflects the availability on the surface of strong basic (O^{2-}) sites and Lewis acid sites (coordinatively unsaturated Mg^{2+} sites) to stabilize the CO_3^{2-} species thus formed [35]; (ii) formation of bicarbonate species may account, moreover, for the availability of basic surface OH^- groups; and (iii) the likely formation of bulk-like carbonate species can further support attribution of the absorption of the acidic CO_2 molecules to the MgO basicity.

3.2.2. Ac/MgO

IR spectra taken of irreversibly adsorbed species of Ac molecules on MgO at various temperatures are shown in Fig. 4A, and the corresponding gas phase spectra are given in Fig. 4B. The RT spectrum monitors a set of IR absorptions (at 1705–1572 cm^{-1}) due to νC=O vibrations and another set occurring at lower frequencies (at 1469–1365 cm^{-1}) assignable to relevant δC–H/νC–O/νC–C vibrations [50]. According to Bellamy [45], νC=O vibration frequency of monocarbonyl ketones is very much influenced by the ketone physical state, intra- and intermolecular associations with adjacent polar groups, and conjugation with olefinic groups. Thus, the νC=O frequency of free Ac molecules in the gas phase (normally occurring around 1740 cm^{-1}) has been shown [45] to suffer a red shift (to 1725–1700 cm^{-1}) upon liquefaction, and further red shifts upon coordination to an acidic center (to 1630 cm^{-1}), intramolecular interaction with adjacent OH groups (to 1600 cm^{-1}), and conjugation with adjacent olefinic groups (to 1550 cm^{-1}). Accordingly, and in the light of previous reports by Zaki et al. [50] and Panov and Fripiat [51], νC=O absorptions at 1705 and 1638 cm^{-1} can be considered to be indicative of coordination of Ac molecules ($((CH_3)_2C{=}O \rightarrow Mg^{2+}$) to differently coordinatively unsaturated Lewis acid sites (five- and four-fold coordinated Mg^{2+}), and the νC=O absorptions at 1616 and 1572 cm^{-1} to coordination of Ac condensation products of diacetone alcohol ($((CH_3)_2C(OH){-}CH_2(CH_3)C{=}O \rightarrow Mg^{2+}$) and mesityl oxide ($((CH_3)_2C{=}CH{-}(CH_3)C{=}O \rightarrow Mg^{2+}$). It is worth noting that Fouad et al. [52] have observed the occurrence of an aldol-condensation-type of reaction of Ac molecules on pure and doped magnesia surfaces, and attributed the reaction to the surface basicity and the stabilization of the reaction products to the availability on the surface of Lewis acid sites.

When the temperature is increased to 200 °C, the spectrum obtained (Fig. 4A) reveals the disappearance of most of the absorptions observed at RT and the emergence, instead, of two strong absorptions (at 1581 and 1423 cm^{-1}) assignable, respectively, to ν_{as} and $\nu_s COO^-$ vibrations of surface acetate species. On the other hand, the spectrum obtained following heating of Ac/MgO at the higher temperature of 400 °C (Fig. 4A) shows the frequency range examined to be dominated by an ill-defined, very strong and broad absorption exhibiting maxima at 1558, 1449, 1352, and 1274 cm^{-1}. These considerable modifications at 400 °C may well be ascribed to the formation of surface/bulk carbonate species, most probably as a result of the adsorption/absorption of CO_2 molecules produced at the expense of decomposing surface acetate species [53]. These and the above results indicate: (i) chemisorption of Ac molecules and their subsequent surface (condensation) products on MgO at RT; (ii) activation of the RT chemisorbed species for surface oxidation into acetate species at 200 °C; and (iii) formation of surface/bulk carbonate species at 400 °C, as a

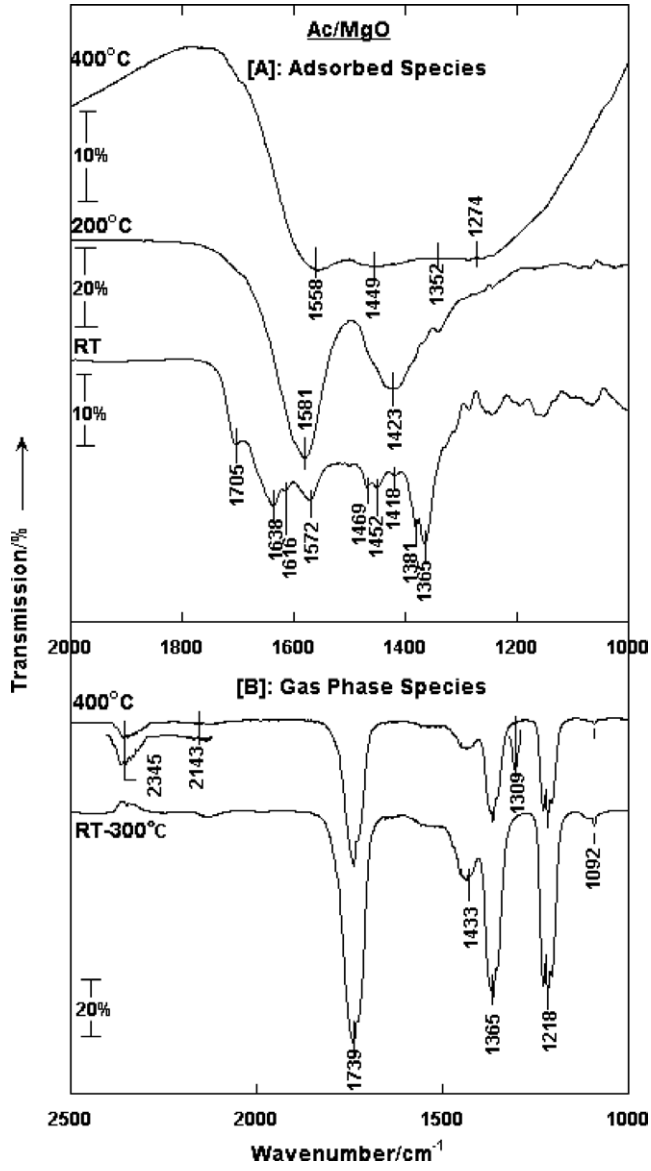

Fig. 4. In situ IR spectra taken at beam temperature of irreversibly adsorbed species (A) and the gas phase (B) of acetone vapour on MgO at the temperatures indicated (in this and the following figures, the adsorbed species spectra (A) were obtained following subtraction of the MgO background spectrum, the gas phase spectra (B) were obtained after subtraction of the cell background spectrum, and the insets are close-ups for the corresponding weak peaks).

result of adsorption/absorption of CO_2 molecules released by decomposing acetate surface species. It is worth noting that all of these primary and secondary surface reactions of Ac molecules are known to be catalyzed by surface basic sites [54]. Thus the occurrence of these condensation reactions reveals that the basic sites exposed on the test magnesia are not only strong, but reactive.

Concomitantly, the spectra taken of the Ac gas phase (Fig. 4B) at RT and following heating up to 300 °C showed nothing but absorptions due to νC=O (at 1739 cm^{-1}) and δC–H/νC–O/νC–C (at 1433, 1365, 1218 cm^{-1}) vibrations of Ac molecules [54]. The absorption intensities remained unchanged even from RT to 300 °C. Only as the temperature reached 400 °C did the spectrum obtained (Fig. 4B) exhibit a detectable intensity loss for the Ac absorptions, as well as the emergence of weak absorptions due to CO_2 (at 2345 cm^{-1}), CO (at 2143 cm^{-1}), and CH_4 (at 1309 cm^{-1}) molecules [54]. The CO_2 and CH_4 molecules are possible decomposition products of surface acetate and carbonate species [53,54], and the formation of minute amounts of CO molecules may indicate the pyrolysis of a small proportion of the Ac molecules [7]. The other expected pyrolytic products of Ac (ketene) [7] are hardly detectable in IR spectra dominated by strong characteristic absorption of Ac molecules [45].

3.2.3. MBOH/MgO

Fig. 5A compares IR spectra taken of MBOH ($(CH_3)_2C(OH)C{\equiv}CH$) adsorbed species on MgO from RT to 400 °C. The RT spectrum monitors a composite, broad absorption (centered around 3656 cm^{-1}) due to νOH vibrations of associated (hydrogen-bonded) hydroxyl groups, involving Mg–OH groups (responsible for the absorption initially at 3749 cm^{-1}) and the alcohol–OH groups. It exhibits, moreover, two twin absorptions at 3307 and 3214 cm^{-1} assignable to νCH vibrations of acetylenic groups bound to the surface in two different modes [55,56]: (i) via interaction of the triple-bond π-electrons with Lewis acid sites ($HC{\equiv}\ldots Mg^{2+}$), and (ii) via interaction of the acetylenic hydrogen with strong Lewis base sites ($\equiv CH\ldots O^{2-}$), respectively. It also displays νCH_3 absorptions (at 2985, 2936, and 2865 cm^{-1}) and δCH/νC–O/νC–C absorptions (at 1474–1087 cm^{-1}) of alkoxide (methylbutynoxide) species [55]. Hence, the RT spectrum reveals that adsorptive interactions at the MBOH/MgO interface results in alcohol-irreversible, dissociative adsorption (the following equations) and nondissociative adsorption via hydrogen bonding to the surface:

$$MBOH_{(g)} + Mg^{2+}_{(s)} + O^{2-}_{(s)} \rightarrow MBO^{-}\ldots Mg^{2+}_{(s)} + HO^{+}_{(s)} \quad (1)$$

and/or

$$MBOH_{(g)} + Mg^{2+}_{(s)} + HO^{-}_{(s)} \rightarrow MBO^{-}\ldots Mg^{2+}_{(s)} + H_2O_{(s)}, \quad (2)$$

where g = gas and s = surface. The tiny but distinct absorption displayed in the RT spectrum at 1638 cm^{-1} may account for δOH vibrations of surface water molecules, thus giving preference to the alkoxide formation via Eq. (2).

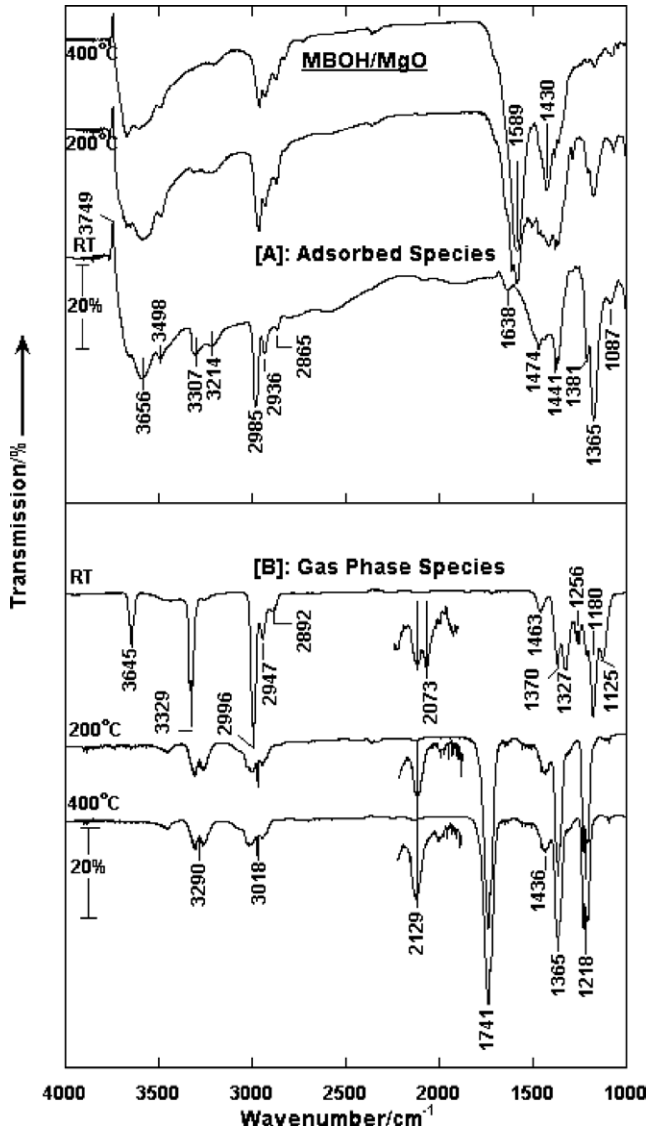

Fig. 5. In situ IR spectra taken at beam temperature of irreversibly adsorbed species (A) and the gas phase (B) of methylbutynol on MgO at the temperatures indicated.

At higher temperatures ($\geqslant$ 200 °C), the spectra obtained (Fig. 5A) indicate a gradual oxidative decomposition of the RT dissociatively and nondissociatively adsorbed species of MBOH, leading eventually to the formation of acetate surface species. The antisymmetric and symmetric νCOO vibrations occurring respectively at 1589 and 1430 cm^{-1} characterize these high-temperature surface species. It is obvious from these results that both the RT and high-temperature adsorptive interactions of MBOH with MgO are driven by the oxide basic sites (OH^- and O^{2-}), whereas Lewis acids stabilize the resulting adsorbed species (MBO^- and CH_3COO^-).

The corresponding gas-phase spectra (Fig. 5B) indicate almost complete catalytic decomposition of MBOH molecules at $\geqslant$ 200 °C; the diagnostic absorptions of the alcohol observed in the RT spectrum (νOH at 3645 cm^{-1}, νCH$\equiv$ at 3329 cm^{-1}, and νCH_3 at 2996–2892 cm^{-1} [55]) are

completely absent from the $\geqslant 200\,^{\circ}C$ spectra. Instead, the high-temperature spectra display diagnostic absorptions of acetylene ($\nu CH\equiv$ at 3290 cm^{-1} and $\nu C\equiv C$ at 2129 cm^{-1} [45]) and Ac ($\nu C{=}O$ at 1741 cm^{-1}) molecules. According to Lauron–Pernot et al. [57], the catalytic decomposition of MBOH into Ac and acetylene molecules is indicative of the exposure on the surface of strong basic sites.

3.2.4. AcOOH/MgO

IR spectra taken of surface species resulting from AcOOH adsorption on MgO between RT and 200 °C (Fig. 6A) are very similar in showing elimination of the νOH absorption (at 3749 cm^{-1}) of surface Mg–OH groups, displaying, instead, a broad νOH absorption (around 3612 cm^{-1}) of associated OH groups, and another νOH absorption (3481 cm^{-1}) due, most probably, to isolated AcOOH molecules. They also similarly monitor a set of three very strong absorptions; two of these are evidently broad (at 1594 and 1436 cm^{-1}), and the third (at 1349 cm^{-1}) is very sharp. The three of them are due to νCOO^{-} vibrations of acetate groups; the two broad ones are reminiscent of surface acetates [5], whereas the sharp one is due to $\nu_s COO^{-}$ of bulk acetates (Fig. 1). The higher-frequency $\nu_{as} COO^{-}$ absorption is most probably shrouded by the two broad absorptions [45]. The weak absorptions at 1245 cm^{-1} and the two very sharp absorptions at 1054 and 1032 cm^{-1} are similar to those displayed for δCH/νC–O/νC–C vibrations of bulk acetates (Fig. 1). Admittedly, however, one cannot exclude with certainty a contribution from δOH vibrations of nondissociatively adsorbed AcOOH molecules to the absorption at 1245 cm^{-1} [42]. νCH_3 vibrations relevant to these various types of AcOOH adsorbed species are shown to absorb IR at 3012–2936 cm^{-1}.

Hence, the spectra obtained between RT and 200 °C support conclusions regarding the adsorption of AcOOH on MgO in two different modes: (i) nondissociative adsorption in the form of hydrogen-bonded AcOOH molecules more abundantly at RT (Eq. (3)) and (ii) dissociate adsorption in the form of surface acetate groups (Eq. (4)). Moreover, they indicate absorption of AcOOH molecules, leading eventually to the formation of bulk acetates (Eq. (5)), as shown by the following equations:

$$CH_3COOH_{(g)} + Mg\text{–}OH_{(s)} \rightarrow CH_3\overset{\overset{O}{\|}}{C}\text{–}O\overset{H}{\diagup}\!\cdots\!\cdots HO\text{–}Mg_{(s)}, \tag{3}$$

$$CH_3COOH_{(g)} + Mg^{2+}_{(s)} + O^{2-}_{(s)} \rightarrow CH_3COO^{-}\ldots Mg^{2+}_{(s)} + HO^{-}_{(s)}, \tag{4}$$

$$2CH_3COOH_{(g)} + MgO_{(b)} \rightarrow Mg(CH_3COO)_{2(b)} + H_2O, \tag{5}$$

where b = bulk. When the temperature is increased to 400 °C, the spectrum obtained (Fig. 6A) indicates persistence of the νCOO^{-} absorptions of surface acetates (at 1594 and 1430 cm^{-1}) with considerable band narrowing, and a marked weakening of the absorptions due to bulk acetates (at 1349, 1245, 1054, and 1032 cm^{-1}). The concomitantly considerably weakened νCH_3 absorptions (at 3012–2936 cm^{-1}) may owe most of their existence to the bulk rather than surface acetates. It is worth admitting that contributions of νOCO vibrations of bulk and/or surface carbonate species to the strong absorptions of the band structure at < 1750 cm^{-1} cannot be totally ruled out.

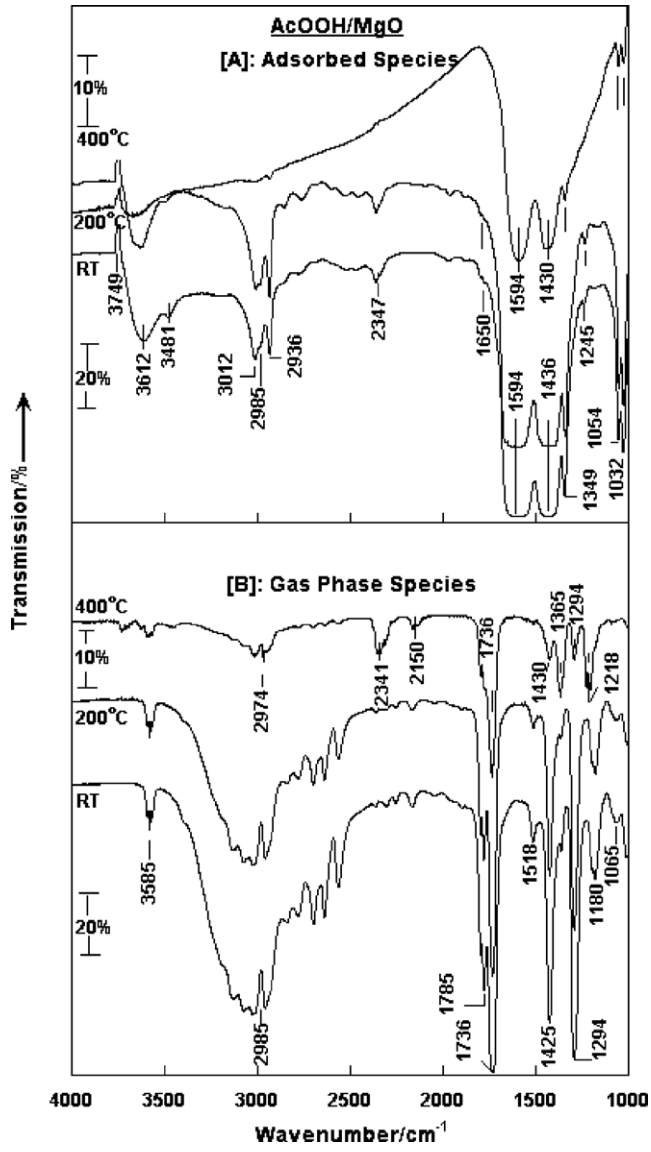

Fig. 6. In situ IR spectra taken at beam temperature of irreversibly adsorbed species (A) and the gas phase of acetic acid on MgO at the temperatures indicated.

The corresponding gas-phase spectra (Fig. 6B) reveal the persistence of diagnostic absorptions of free and dimerized AcOOH molecules with heating to 200 °C: νOH at 3585 cm^{-1} (free), νOH at 2985 cm^{-1} (dimerized), $\nu C{=}O$ at 1785 cm^{-1} (free), $\nu C{=}O$ at 1736 cm^{-1} (dimerized), and δC–H/νC–O/νC–C at 1518–1065 cm^{-1} (free and dimerized) [45]. When the temperature is increased to 400 °C, that is, to the temperature where decomposition of bulk ac-

etates is made prominent (Fig. 6A), the gas-phase spectrum obtained (Fig. 6B) indicates drastic weakening of the acid absorption, with emergence of characteristic absorptions of Ac (at 2974, 1736, 1430, 1365, and 1218 cm^{-1}; cf. Ac diagnostic spectra in Fig. 4B), CO_2 (at 2341 cm^{-1}), and CO (at 2150 cm^{-1}) molecules. These results were observed, but weakly, in a gas-phase spectrum obtained following heating at 300 °C (not shown). Accordingly, one can conclude that the onset of AcOOH ketonization, both pyrolytically (via bulk acetates) and catalytically (via surface acetates), commences near 300 °C.

3.3. AcOOH ketonization

3.3.1. Reaction behavior

Fig. 7 illustrates the reaction behavior of AcOOH over MgO as observed chromatographically in a flow reactor (Fig. 7A) and IR-spectroscopically in a static reactor (Fig. 7B). The amount of AcOOH and its detectable products (Ac and CO_2) are graphically presented as a function of temperature in Fig. 7A, and as a function of time at 300 °C in Fig. 7B. Separation and estimation of water among the products was not feasible with the analytical techniques applied. However, two important observations may signify its formation: (i) the display of IR absorptions due to bending (at 1650 cm^{-1}) and stretching (at 3612–3400 cm^{-1}) vibrations of O–H bonds of hydrogen-bonded and coordinated H_2O molecules in spectra taken of adsorbed species established on the catalyst during the reaction (Fig. 6A), and (ii) the observed product/reactant proportions (Fig. 7A), which do not fit the reaction stoichiometry [5,7]

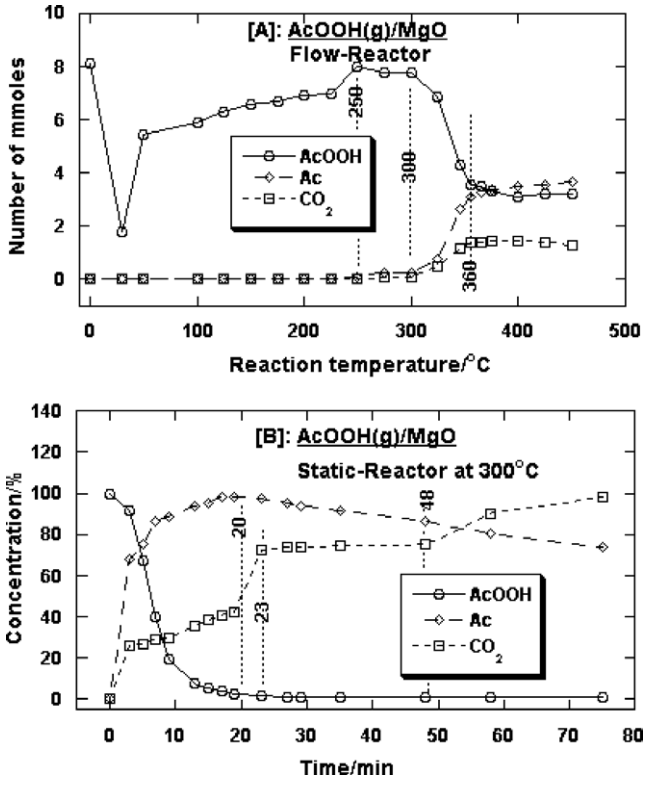

Fig. 7. Composition of the reaction mixture of acetic acid ketonization over MgO in a flow-reactor as a function of temperature (A), and in a static-reactor (at 300 °C) as a function of time.

$$2CH_3COOH \rightarrow CH_3COCH_3 + CO_2 + H_2O, \quad (6)$$

unless production of water is considered.

Fig. 7A demonstrates a sudden, considerable consumption of the amount of the acid when it is allowed to flow over the catalyst near RT, without detectable release of products. Hence, it is due solely to uptake by the catalyst surface and bulk, as evidenced by the IR spectra shown in Fig. 6A. This behaviour is shown to continue to occur, but to a lesser extent, at higher temperatures up to about 250 °C, where the amount led of the acid is shown to remain unchanged. Fig. 7A reveals three different temperature-dependent behaviors at higher temperatures: (i) at 250–300 °C, a mild consumption of the acid, corresponding to a minute production of Ac and CO_2; (ii) at 300–360 °C, a steep, considerable consumption of the acid, corresponding to a proportional increase in the amounts of the products, particularly of the Ac molecules; and (iii) at $>$ 360 °C, a steady consumption of the acid, and a corresponding steady production of Ac and CO_2. When it is correlated with results conveyed by the IR spectra shown in Fig. 6, one may relate the accelerated ketonization at 300–360 °C to the observed decomposition of the catalyst bulk acetate species, which has been formed, together with surface acetates, at the lower temperature regime. Thus, the steady ketonization reached at $>$ 360 °C can be considered to be indicative of pure catalytic ketonization, in which the surface reactions are the key player and the composition of the reaction mixture is thermodynamically controlled. The observed destabilization of bulk magnesium acetate and the intermediate bulk carbonate at $>$ 300 °C (Figs. 2, 3, and 6) lends strong support to the temperature-dependent reaction behavior described above.

The time-dependent reaction behavior at 300 °C (Fig. 7B), the temperature at which bulk acetate and carbonate species commence to decompose, indicates a steep consumption of almost 80% of the acid within the first 10 min of the reaction lifetime, followed by a slow consumption of the remaining amount (20%) over the following 10 min. Correspondingly, both Ac and CO_2 are produced in different magnitudes but display similar time-dependent behaviors. As the amount of Ac is shown to shoot up to ca. 60% within the first 2 min, the amount of CO_2 also steeply increases, reaching 20%. Afterward, the amount of Ac continues to increase, though gradually, reaching almost 100% after the elapse of 20 min of the reaction, and the amount of CO_2 also undergoes a gradual increase, up to ca. 40%, over the same time. At $>$ 20 min, the time-dependent behaviors of the amounts of Ac and CO_2 are different. Whereas the amount of Ac undergoes a continuous but gradual decrease with time, dropping back to ca. 70% after the elapse of 75 min, the amount of CO_2 shows, conversely, a two-step increase, reaching 100% over the same period of time. In the first step, at 20–23 min,

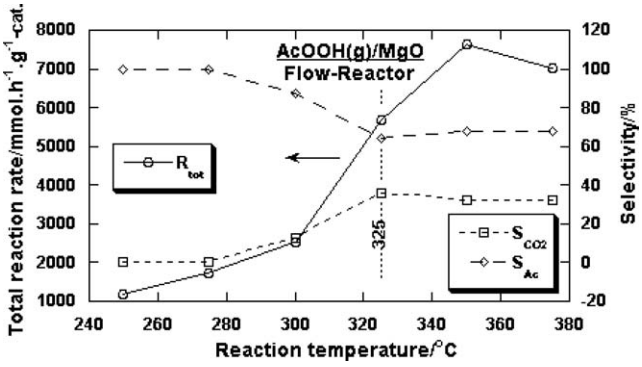

Fig. 8. Reaction rate and selectivity of acetic acid ketonization over MgO as a function of temperature.

the amount of CO_2 jumps from 40 to 75% and then remains almost constant until the elapse of ca. 50 min, where the second step commences, gradually increasing the amount of CO_2, to 100%.

Recall that at 300 °C, the temperature at which bulk magnesium acetate is at the verge of thermal destabilization, the isothermal consumption of AcOOH (Fig. 7B) can still be attributed to its joint catalytic and pyrolytic ketonization. The almost complete consumption of AcOOH within the first 10 min may be attributed to both adsorption and absorption of its molecules by the catalyst. On the other hand, the time-dependent production behaviors of Ac and CO_2 should also account for their further surface reactions. Accordingly, the gradual decrease in Ac at > 20 min can be correlated well with the IR results shown in Fig. 4. In other words, the loss in concentration of Ac can be ascribed to its adsorption, and subsequent aldol-condensation-type of reaction and oxidation into surface acetates, as monitored in the spectra shown in Fig. 4A. These adsorptive interactions may lead to a release of CO_2 into the gas phase, following the establishment of equilibrium concentration of CO_2 over a wide range of time (23–48 min), which may explain the second step in the production of CO_2 (at > 50 min, Fig. 7B). The first step (20–23 min, Fig. 7B), on the other hand, may be ascribed to CO_2 production at the expense of formation and subsequent decomposition of carbonate species (Fig. 3). This may explain the early low (nonstoichiometric) production of CO_2.

3.3.2. Reaction rate and selectivity

Fig. 8 demonstrates the total reaction rate (mmol h^{-1} g_{cat}^{-1}) and selectivity (%) obtained for AcOOH ketonization over MgO as a function of temperature in the flow reactor. It is obvious from the results that the reaction commences near 250 °C at a moderate rate until the temperature of 300 °C is reached. At this temperature range, the Ac selectivity of the reaction is markedly higher than the CO_2 selectivity. When the reaction temperature is increased, the reaction rate is steeply enhanced, reaching a maximum value near 350 °C. In the meantime, the Ac and CO_2 selectivities of the reaction converge, reaching their closest approach near 325 °C, and remain as close over the higher temperature regime. Thus, both the dramatic change in the reaction rate and the independent changes in the reaction selectivity are compatible with the observed changes of the reaction behaviors as a function of temperature (Fig. 7A), accounting for the occurrence of two different types of ketonization reaction. This is in the sense that the production of Ac and CO_2 from one and the same reaction route would have been reflected in one and the same pattern of Ac and CO_2 selectivity change as a function of temperature.

3.3.3. Reaction type

The reaction behavior, rate, and selectivity changes described above imply the occurrence of acid ketonization over MgO via two overlapping routes: the pyrolytic and catalytic routes. In the pyrolytic route, AcOOH molecules are absorbed, leading to the formation of bulk magnesium acetate (Eq. (5)), which is, subsequently, thermally decomposed, releasing Ac and CO_2 molecules into the gas phase. In the catalytic route, on the other hand, AcOOH molecules are dissociatively adsorbed in the form of surface acetates (Eq. (4)), which are activated on the surface for conversion into gas-phase Ac, CO_2, and H_2O molecules. The formation and subsequent decomposition of bulk and/or surface carbonate species in the pyrolytic or the catalytic route may also be assumed to indicate intermediate precursor species for the production of CO_2 molecules. Therefore, bulk magnesium acetate and carbonate compounds were thermally analyzed, and their solid- and gas-phase decomposition products were chromatographically and spectroscopically identified and quantified, in an attempt to characterize reaction events and products involved in the pyrolytic route. Consequently, it is hoped that those involved in the catalytic route may be discerned.

Fig. 9 exhibits TG (and corresponding DTG) curves obtained for bulk $MgCO_3$ (Fig. 9A) and its physical mixture with bulk $Mg(CH_3COO)_2 \cdot 4H_2O$ (Fig. 9B) in an air atmosphere. The Fig. 9B inset, moreover, shows a DTG curve obtained (at 300–400 °C) for the acetate compound only, in a nitrogen atmosphere. The results presented in Fig. 9A show the magnesium carbonate compound to decompose in two steps maximized at 250 and 438 °C in the air atmosphere. In the same atmosphere, the mixture of the carbonate and acetate compounds gave rise to TG and DTG curves, resolving the previously observed decomposition steps of the acetate compound (Fig. 2C) as occurring at almost the same temperatures (82, 130, and 357 °C) and the major decomposition step of the carbonate compound as occurring at almost 100 °C less than the pure compound (i.e., at 336 instead of 438 °C; Fig. 9A). This indicates beyond doubt that in the coexistence of acetate bulk species the decomposition of the carbonate bulk species is markedly enhanced. Eventually, the carbonate compound, which is thermally more stable than the acetate compound, decomposes just a bit earlier than the acetate compound ($T_{max} = 336$ and 357 °C). Thus, when they coexist, the decomposition courses of the carbonate and acetate compounds overlap.

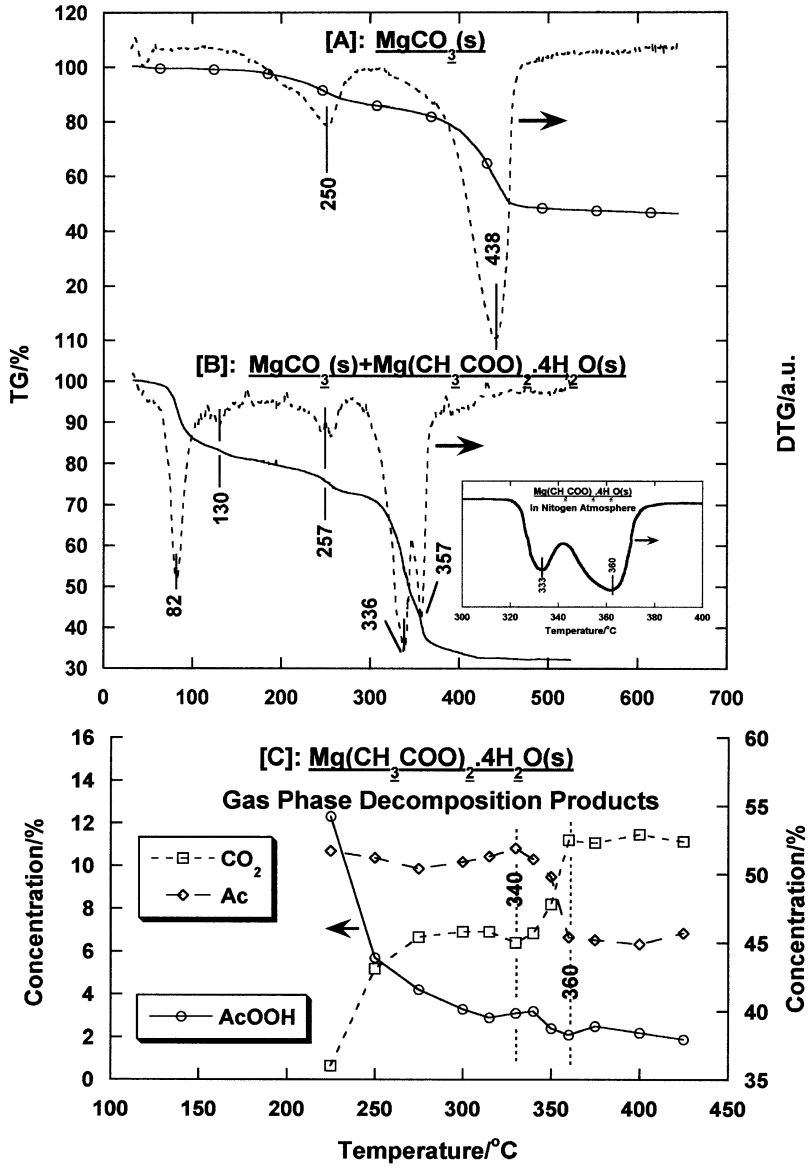

Fig. 9. TG (and DTG) curve obtained on heating (at 20 °C/min) small portions (10–15 mg) of bulk magnesium carbonate (A) and its physical mixture with bulk magnesium acetate (B) in the atmosphere of air (50 cm^3/min) (the inset DTG curves was obtained in nitrogen atmosphere), and GC-determined concentration of the indicated (C) gas phase decomposition products of the magnesium acetate as a function of temperature.

When carried out in an nitrogen atmosphere, the thermal decomposition of the acetate compound is shown (Fig. 9B, inset) to exhibit two mass loss steps maximized at 333 and 360 °C. The low-temperature step is assigned to decomposition of the acetate into carbonate, whereas the high-temperature step is assigned to decomposition of the latter into MgO. The relative magnitudes of mass losses undertaken via the two steps are closer to that shown for the mixture of acetate and carbonate (Fig. 9B) than that observed for the pure acetate compound (Fig. 2C) when it is decomposed in air. These results indicate that the formation of intermediate carbonate compound during the acetate decomposition into MgO is considerably hampered in the presence of an oxygen (air) atmosphere.

In line with the results presented in Figs. 2 and 9 (A and B), in situ IR spectra taken of the gas phase surrounding a sample of $Mg(CH_3COO)_2 \cdot 4H_2O$, which has decomposed inside the IR cell upon heating to 480 °C, are compared in Fig. 10. The spectra taken from RT to 200 °C are similar in displaying nothing but diagnostic absorptions of dimerized AcOOH molecules (see Fig. 6B for authenticity). At 250–400 °C, the spectra show the AcOOH absorptions to weaken gradually, with the emergence of diagnostic absorptions of Ac (at 1368, 1218, and 1092 cm^{-1}) and CO_2 (at 2336 cm^{-1}) molecules. At the higher temperature of 480 °C, the spectrum obtained monitors the emergence of detectable absorptions due to CO (at 2150 cm^{-1}) and CH_4 (at 3016 and 1308 cm^{-1}) molecules, largely at the expense

of some Ac molecules. Hence, the detectable, primary gas-phase decomposition products of the test acetate compound are AcOOH, Ac, and CO_2 molecules.

Fig. 9C shows variation of the concentration (%) of the gas-phase decomposition products (AcOOH, Ac, and CO_2) of the bulk acetate compound as a function of the decomposition temperature. The results indicate, in line with those exhibited in Fig. 10, that the release of detectable amounts of the products occurs near 225 °C, that is, following dehydration of the acetate ($Mg(CH_3COO)_2 \cdot 4H_2O$, Fig. 2C). At higher temperatures, the amount of AcOOH decreased steeply at 225–250 °C, but gradually at > 250 °C. In contrast, the amount of Ac remained largely unchanged up to 340 °C, when it decreased steeply to an almost constant value until it reached a temperature of 425 °C. On the other hand, the amount of CO_2 increased steeply with temperature up to 250 °C, then gradually up to a constant value with a further temperature increase to 340 °C. Above 340 °C, the amount of CO_2 increased steeply again, reaching another constant value at 360 °C.

The above results (Fig. 9C) may help us to characterize the pyrolytic course of AcOOH ketonization. It is shown to commence near 225 °C by the production of Ac and CO_2, where the latter product is initially markedly taken up by freshly generated MgO particles to form, most likely, bulk and/or surface carbonate species (Fig. 3). Near 340 °C, the Ac molecules are markedly used up in adsorption and surface reactions as the generation of MgO is, expectedly, considerably enhanced around this temperature (Fig. 2C). MgO is most probably formed at the expense of intermediate carbonate compound (the product of CO_2 absorption). Thus, the observed upsurge in the production of CO_2 at 340–360 °C must have been associated with the thermal decomposition of the intermediate carbonate compound. These conclusions are supportive of suggestions put forward [7] regarding the concurrence of pyrolytic ketonization during the catalytic ketonization of AcOOH on MgO.

3.3.4. Reaction mechanism

The results presented above provide strong indications of the ketonization of AcOOH vapour over MgO both pyrolytically and catalytically at $\geqslant 225$ °C. The pyrolytic route commences at 225 °C after the absorption of AcOOH molecules and the formation of bulk magnesium acetate species, which occurs readily and quantitatively (in 2 h) near RT, as described by Eq. (5). It involves, most likely, the formation and subsequent decomposition of intermediate bulk and/or surface carbonate species, as depicted in the following reaction pathways:

$$Mg(CH_3COO)_{2(b)} \xrightarrow{\mathbf{I}} CH_3COCH_{3(g)} + MgCO_{3(b)}$$
$$\xrightarrow{\mathbf{II}} CH_3COCH_{3(g)} + CO_{2(g)} + MgO.$$

The strong MgO tendency toward AcOOH absorption (Fig. 2B) is motivated primarily by the strong basicity (ionicity) of the oxide. Of course, the known dehydration activity of MgO [58] would also promote the acid absorption. The ketonization pathway I finds stronger support from the present results than the pathway II.

On the other hand, the catalytic ketonization is shown to occur detectably at $\geqslant 300$ °C, probably after the advance of the pyrolytic ketonization and the consequent generation of free MgO surfaces. The initial step of the reaction seems to be the adsorptive interaction of AcOOH molecules with MgO surfaces, leading to the formation of surface acetate species (Eq. (4)). Subsequently, the catalytic ketonization route may involve the following reaction pathways:

$$2CH_3COO^- \ldots Mg^{2+}_{(s)} + 2OH^-_{(s)}$$
$$\xrightarrow{\mathbf{I}} CH_3COCH_{3(g)} + CO_{2(g)} + H_2O_{(g)} + 2Mg^{2+}_{(s)} + 2O^{2-}_{(s)}$$
$$\xrightarrow{\mathbf{II}} CH_3COCH_{3(g)} + CO_3{}^{2-} \ldots (Mg^{2+})_{2(s)} + H_2O_{(g)} + O^{2-}_{(s)}.$$

The IR evidence for the involvement of isolated Mg–OH groups (Fig. 5A) lends strong support to the suggestion of their contribution to surface reactions of the adsorbed acetate species, leading to either pathway I or pathway II. Compatibly, studies performed on the transformation of benzaldehyde, via a Cannizaro-type reaction, into benzyl alcohol on MgO surfaces have been assumed by Haffad et al. [59] to indicate the high reactivity and mobility of Mg–OH groups. Moreover, IR spectra obtained by Malinowski et al. [60] for steamed and deuterated MgO showed the persistence of free and combined surface Mg–OH, with heating to 600 °C, and the persistence of the combined Mg–OH with further heating to 1300 °C. The present results, indicating the thermal instability of surface carbonate species at > 300 °C (Fig. 3), may also indicate pathway I over pathway II.

Pestman et al. [7] have assessed general mechanisms proposed [61–63] for surface reactions involved in the catalytic ketonization of carboxylic acids. Based on their own experimental results and some thermodynamic considerations, these authors have reached the following conclusions: (i) the formation of ketene and ketenic-like ($RR'C{=}C{=}O$) intermediates in the reaction course may be excluded; (ii) abstraction of α-hydrogen atoms from the acid molecule, or acetate surface species, is an essential step in the reaction course; (iii) the alkylidene carboxylate thus formed, oriented parallel to the surface, reacts with nearby carboxylate species and a hydrogen atom to give the ketone; and (iv) the remaining carboxyl groups form CO_2. Although the present results can neither prove nor disprove these conclusions, they can stress the importance of surface carboxylate (acetate) species for the reaction and exclude the formation of ketene and ketenic-like species, at least at a detectable level, throughout the reaction. The observed formation of minority CH_4 and CO molecules, which have been considered [61–63] to be indicative of the contribution of ketene and ketenic-like species to the reaction, is confined to the upper tempera-

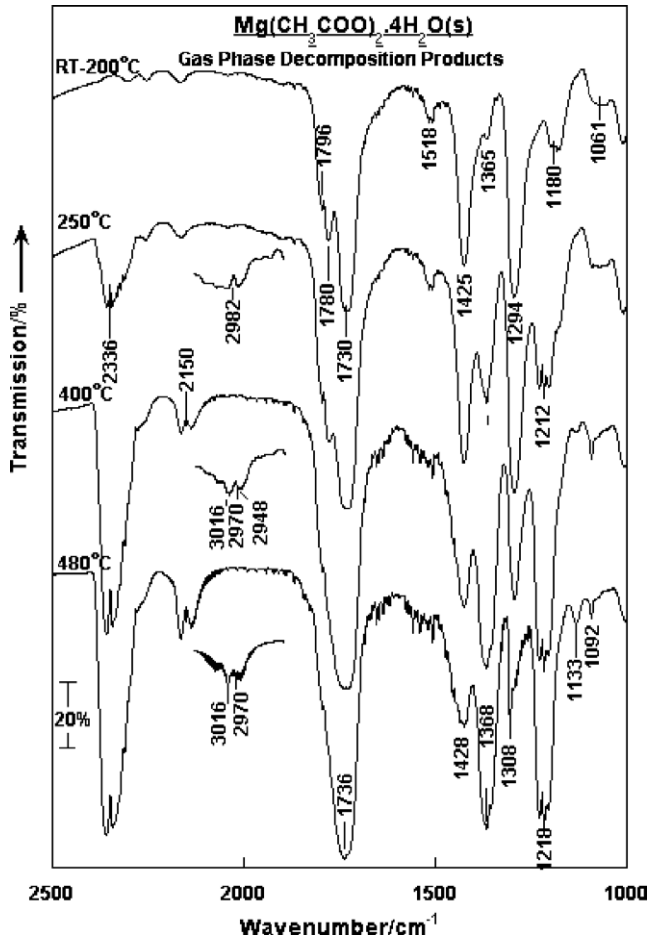

Fig. 10. In situ IR spectra taken at beam temperature of the gas phase decomposition products of bulk magnesium acetate at the temperatures indicated (the insets are corresponding νCH peaks).

ture regime ($\geqslant 400\,^{\circ}C$) of the reaction (Fig. 10). Hence, they could well be considered to be pyrolytic products of the Ac produced [54].

However, most of the observed consumption of Ac molecules over MgO at $\geqslant 300\,^{\circ}C$ (Fig. 7B) is due to its adsorption and further surface reactions (Fig. 4). In a previous investigation [54] focusing on the surface chemistry of Ac on metal oxides, it was found that upon coordination to Lewis acid sites, Ac molecules are activated for aldol-condensation-type reactions. Accordingly, the following surface reaction pathways may be suggested to undertake the observed conversion of Ac molecules into the observed surface condensation products (Fig. 4A):

$$(CH_3)_2C{=}O\ldots Mg^{2+}_{(s)} + {}^{-}HO\ (\text{or } O^{2-})_{(s)} \rightarrow \underset{\text{enolate}}{CH_2{=}C(CH_3){-}O^{-}\ldots Mg^{2+}_{(s)}} + H_2O\ (\text{or } {}^{-}HO)_{(s)},$$

$$(CH_3)_2C{=}O\ldots Mg^{2+}_{(s)} + CH_2{=}C(CH_3){-}O^{-}\ldots Mg^{2+}_{(s)} + {}^{+}H_2O_{(s)} \rightarrow \underset{\text{diacetone alcohol}}{(CH_3)_2C(OH){-}CH_2{-}(CH_3)C{=}O\ldots Mg^{2+}_{(s)}} + HO\ldots Mg^{2+}_{(s)},$$

$$(CH_3)_2C(OH){-}CH_2{-}(CH_3)C{=}O\ldots Mg^{2+}_{(s)} + \square_{(s)} \rightarrow \underset{\text{mesityl oxide}}{(CH_3)_2C{=}CH{-}(CH_3)C{=}O\ldots Mg^{2+}_{(s)}} + H_2O_{(s)},$$

where $\square_{(s)}$ stands for reactive surface vacancy. Neither of the Ac condensation products above indicated was released into the gas phase. They are stabilized on the surface and, at high temperatures, oxidized into surface acetate and carbonate species (Fig. 4A).

4. Conclusion

The results presented and discussed here indicate that the ketonization of acetic acid vapour over MgO into Ac, CO_2, and H_2O occurs not only catalytically, but also pyrolytically when MgO is converted partially or totally into bulk magnesium acetate at RT. The initial interactions of AcOOH molecules with MgO are both adsorptive and absorptive. The AcOOH absorption and the consequent formation of bulk magnesium acetate species are promoted by the evident, strong basicity (ionicity) of MgO, despite its high lattice energy (Mg–O bond strength) [7]. The bulk acetate thus formed decomposes at $\geqslant 225\,^{\circ}C$ into Ac, CO_2, and H_2O. The CO_2 may be a direct product of the acetate decomposition, or a decomposition product of intermediate bulk and/or surface carbonate species at higher temperatures. On the other hand, the AcOOH adsorption results in the formation of surface acetate species, which are activated on the surface at $\geqslant 300\,^{\circ}C$ to ketonization into Ac, CO_2, and H_2O. The surface activation seems to require a synergy of acid-base surface sites. The Ac molecules are adsorbed to MgO and are thereby activated for further aldol-condensation-type surface reaction. The condensation products are stabilized on the surface and hence are not desorbed into the gas phase. Instead, they are oxidized into surface acetate and carbonate species.

Acknowledgment

M.I.Z. acknowledges with appreciation an equipment donation (V-8151/03042) by the Alexander von Humboldt Foundation (Bonn, Germany) that made possible a necessary rehabilitation of the IR reactor cell used in the present investigation.

References

[1] J.C. Kuriacose, Metals Miner. Rev. 9 (1970) 5.
[2] R. Klimkiewicz, H. Grabowska, A. Biskupski, L. Sypek, E. Fabisz, I. Morawski, Chemia 142 (2001) 53.
[3] R. Klimkiewicz, H. Teterycz, H. Grabowska, I. Morawski, L. Syper, B. Licznerski, J. Am. Oil Chem. Soc. 78 (2001) 533.
[4] N.P. Matsota, V.D. Mezhov, Zh. Prikl. Khim. (Leningrad) 50 (1977) 2061.
[5] M.A. Hasan, M.I. Zaki, L. Pasupulety, Appl. Catal. A 243 (2003) 81.

[6] S.A. Halawy, Monatshefte f. Chem. 134 (2003) 371.
[7] R. Pestman, R.M. Koster, A. van Duijne, J.A.Z. Pieterse, V. Ponec, J. Catal. 168 (1997) 265.
[8] K.M. Parida, A. Samal, N.N. Das, Appl. Catal. A 166 (1998) 201.
[9] D.H.R. Barton, B. Hu, D.K. Taylor, R.U. Rojas Whal, Tetrahedron Lett. 37 (1996) 1133.
[10] S.M. Fleming, T.A. Robertson, G.J. Langley, T.D. Bugg, Biochem. 39 (2000) 1522.
[11] E. Mueller-Erlwein, B. Rosenberger, Chem. Ing. Tech. 62 (1990) 512.
[12] N.P. Matsota, V.D. Mezhov, Z.S. Novocherk, Zh. Prikl. Khim. (Leningrad) 44 (1971) 1823.
[13] G.E. Lienhard, T.-C. Wang, J. Am. Chem. Soc. 91 (1969) 1146.
[14] S. Sugiyama, K. Sato, S. Yamasaki, K. Kawashiro, H. Hayashi, Catal. Lett. 14 (1992) 127.
[15] J.-B. Senderens, Bull. Soc. Chim. 5 (1909) 905.
[16] E.R. Squibb, J. Am. Chem. Soc. 17 (1895) 187.
[17] M. Glinski, M. Kaszubski, React. Kinet. Catal. Lett. 70 (2000) 271.
[18] J.A. Martens, M. Wydoodt, P. Espeel, P.A. Jacobs, Stud. Surf. Sci. Catal. 78 (1993) 527.
[19] Y. Chiang, E.A. Jefferson, A.J. Kresge, V.V. Popik, J. Am. Chem. Soc. 121 (1999) 11330.
[20] J.I.K. Almstead, B. Urwyler, J. Wirz, J. Am. Chem. Soc. 116 (1994) 954.
[21] Y. Ishii, K. Yamawaki, T. Ura, H. Yamada, T. Yoshida, M. Ogawa, J. Org. Chem. 53 (1988) 3587.
[22] O.V. Skvortsova, A.M. Chashchin, E.V. Elizova, V.N. Gusakov, Lesokhim. Prom-sti 25 (1976) 76.
[23] R. Clement, Oleagineux 13 (1958) 101.
[24] The Plastergon Wall Board Co., GB Patent No. GB 478588, 19380120.
[25] I.G. Farbenindustrie A.G., GB Patent No. GB 477499, 19371231.
[26] J.C. Kuriacose, Bull. Soc. Chim. Belgs. 64 (1955) 502.
[27] I.E. Sosnina, S.V. Lysenko, Khim. 14 (1973) 354.
[28] M. Demorest, D. Mooberry, J.D. Danforth, Ind. Eng. Chem. 43 (1951) 2569.
[29] M.I. Zaki, M.A. Hasan, L. Pasupulety, Langmuir 17 (2001) 4025.
[30] V.I. Dyshlovoi, F.V. Linchevskii, B.S. Grinenko, Neftepererab. Neftekhim. (Moscow) 9 (1974) 26.
[31] H. Idriss, K.S. Kim, M.A. Barteau, Stud. Surf. Sci. Catal. 67 (1991) 327.
[32] J.C. Kuriacose, J. Sci. Ind. Research (India) 20B (1961) 82.
[33] K.M. Parida, H.K. Mishra, J. Mol. Catal. A 139 (1999) 73.
[34] H. Knözinger, in: J.-M. Basset, et al. (Eds.), Surface Organometallic Chemistry: Molecular Approaches to Surface Catalysis, Kluwer-Academic, New York, 1988, pp. 35–46.
[35] G.A.H. Mekhemer, S.A. Halawy, A.M. Mohamed, M.I. Zaki, J. Phys. Chem. B (2004) 13379.
[36] G. Busca, Catal. Today 41 (1998) 191.
[37] S. Coluccia, M. Baricco, L. Marchese, G. Martra, A. Zecchina, Spectrochim. Acta 49A (1993) 1289.
[38] A. Zecchina, M.G. Lofthouse, F.S. Stone, J. Chem. Scoc. Faraday Trans. 1 71 (1975) 1476.
[39] M.A. Mohamed, A.K. Galwey, Thermochim. Acta 217 (1993) 263.
[40] International Center for Diffraction Data, 12 Campus Boulevard, Newton Square, PA 19073-3273, USA.
[41] J.B. Peri, R.B. Hannan, J. Phys. Chem. 64 (1960) 1521.
[42] S.A. Halawy, M.A. Mohamed, S.F. Abdel-Hafez, J. Mol. Catal. 94 (1994) 191.
[43] V.I. Yakerson, E.A. Fedorovskaya, A.L. Klyachko-Gurvich, A.M. Rubinstein, Kinet. Katal. 2 (1961) 907.
[44] N.T. McDevitt, W.L. Baun, Spectrochim. Acta 20 (1964) 799.
[45] L.J. Bellamy, The Infrared Spectra of Complex Molecules, Chapman and Hall, London, 1975.
[46] M.I. Zaki, H. Knözinger, Mater. Chem. Phys. 17 (1987) 201.
[47] M.A. Bernard, F. Busnot, Bull. Soc. Chim. Fr. (2000) 1968.
[48] G. Busca, V. Lorenzelli, Mater. Chem. 7 (1982) 89.
[49] C. Morterra, G. Ghiotti, F. Boccuzzi, S. Coluccia, J. Catal. 51 (1978) 299.
[50] M.I. Zaki, M.A. Hasan, L. Pasupulety, Langmuir 17 (2001) 768.
[51] A. Panov, J.J. Fripiat, Langmuir 14 (1998) 3788.
[52] N.E. Fouad, P. Thomasson, H. Knözinger, Appl. Catal. A 196 (2000) 460.
[53] M.I. Zaki, N. Sheppard, J. Catal. 80 (1983) 114.
[54] M.I. Zaki, M.A. Hasan, F.A. Al-Sagheer, L. Pasupulety, Langmuir 16 (2000) 430.
[55] M.A. Hasan, M.I. Zaki, L. Pasupulety, J. Mol. Catal. A 178 (2002) 125.
[56] N.E. Fouad, P. Thomasson, H. Knözinger, Appl. Catal. A 194 (2000) 213.
[57] H. Lauron-Pernot, F. Luck, J.M. Popa, Appl. Catal. 78 (1991) 213.
[58] M.A. Barteau, J.M. Vohs, in: G. Ertl, et al. (Eds.), Handbook of Heterogeneous Catalysis, vol. 2, VCH–Weinheim, 1992, pp. 873–888.
[59] D. Haffad, U. Kameswari, M.M. Bettahar, A. Chambellan, J.C. Lavalley, J. Catal. 172 (1997) 85.
[60] S. Malinowski, S. Szczepanska, J. Sloczynski, J. Catal. 7 (1967) 68.
[61] J.C. Kuriacose, S.S. Jewur, J. Catal. 50 (1977) 330.
[62] F. Gonzalez, G. Munuera, J.A. Prieto, J. Chem. Soc., Faraday Trans. I 74 (1978) 1517.
[63] T. Imanaka, T. Tanemoto, S. Teranishi, in: J.W. Hightower (Ed.), Proceedings of 5th International Congress on Catalysis, Palm Beach, 1972, vol. 1, North-Holland, Amsterdam, 1973, p. 163.